Improved upper limit on the decay $K^+ \to \pi^+ \mu^+ e^-$

Aleksey Sher,[7,*] R. Appel,[3,6] G. S. Atoyan,[4] B. Bassalleck,[2] D. R. Bergman,[6,†] N. Cheung,[3] S. Dhawan,[6] H. Do,[6] J. Egger,[5] S. Eilerts,[2,‡] H. Fischer,[2,‖] W. Herold,[5] V. V. Issakov,[4] H. Kaspar,[5] D. E. Kraus,[3] D. M. Lazarus,[1] P. Lichard,[3] J. Lowe,[2] J. Lozano,[6,¶] H. Ma,[1] W. Majid,[6,**] S. Pislak,[6,7,§] A. A. Poblaguev,[4] P. Rehak,[1] A. Sher,[3,††] J. A. Thompson,[3,‡‡] P. Truöl,[6,7] and M. E. Zeller[6]

[1]*Brookhaven National Laboratory, Upton, New York 11973, USA*
[2]*Department of Physics and Astronomy, University of New Mexico, Albuquerque, New Mexico 87131, USA*
[3]*Department of Physics and Astronomy, University of Pittsburgh, Pittsburgh, Pennsylvania 15260, USA*
[4]*Institute for Nuclear Research of Russian Academy of Sciences, Moscow 117 312, Russia*
[5]*Paul Scherrer Institut, CH-5232 Villigen, Switzerland*
[6]*Physics Department, Yale University, New Haven, Connecticut 06511, USA*
[7]*Physik-Institut, Universität Zürich, CH-8057 Zürich, Switzerland*

(Received 28 January 2005; published 25 July 2005)

Based on results of a search for the lepton-family-number-violating decay $K^+ \to \pi^+ \mu^+ e^-$ with data collected by experiment E865 at the Alternating Gradient Synchrotron of Brookhaven National Laboratory, we place an upper limit on the branching ratio at 2.1×10^{-11} (90% C.L.). Combining the results with earlier E865 data and those of a previous experiment, E777, an upper limit on the branching ratio of 1.3×10^{-11} (90% C.L.) is obtained.

DOI: 10.1103/PhysRevD.72.012005 PACS numbers: 13.20.−v

I. INTRODUCTION

We report on a search for the decay $K^+ \to \pi^+ \mu^+ e^-$ ($K_{\pi\mu e}$). This is a lepton-family-number-violating (LFNV) decay and, thus, is strictly forbidden in the standard model (SM) with massless neutrinos. Incorporating massive neutrinos into the SM, which is required by the growing evidence for the lepton family transformations in the neutrino sector [1], results in a prediction of LFNV kaon decays at an unobservably low level [2]. Thus an observation of a LFNV process like the decay $K_{\pi\mu e}$ would serve as a clear indication of physics beyond the SM. Moreover, extensions of the SM such as extended gauge theories [3,4], technicolor [5], and supersymmetry [6] do allow LFNV processes.

A first search for $K_{\pi\mu e}$, performed during the 1970s, resulted in an upper limit on the decay's branching ratio (B) of 4.8×10^{-9} (90% C.L.) [7]. A search for this decay in the Brookhaven National Laboratory (BNL) was initiated by Experiment 777, in which the upper limit $B < 2.1 \times 10^{-10}$ was established [8]. The data collected in 1995 [9] and 1996 [10,11] by BNL Experiment 865, a successor to E777, allows us to lower the combined upper limit to $B(K^+ \to \pi^+ \mu^+ e^-) < 2.8 \times 10^{-11}$ (90% C.L.) [11]. Nevertheless a null search result is useful since it can either put constraints on the parameters of the existing extension models that allow LFNV or rule them out.

For example, in the extended technicolor model (ETC) [3] the transition between the leptons of different generations can be mediated by a horizontal ETC boson (H). The corresponding diagram, shown in Fig. 1, is similar to the diagram of the familiar decay $K^+ \to \pi^0 \mu^+ \nu$. Using the assumption that H and W boson couplings are approximately equal to each other, one can relate the H boson mass, M_H, to the $K_{\pi\mu e}$ branching ratio [3]:

$$M_H \approx 85 \text{ TeV} \left[\frac{10^{-11}}{B(K^+ \to \pi^+ \mu^+ e)} \right]^{1/4}. \qquad (1)$$

The quoted limit $B(K^+ \to \pi^+ \mu^+ e) < 2.8 \times 10^{-11}$ corresponds to a 65 TeV lower limit on the M_H mass scale. A competitive constraint on the new physics mass scale may be obtained from another LFNV kaon decay, $K_L \to \mu^\pm e^\mp$ ($K_{\mu e}$), for which an upper limit on its branching ratio is set at 4.7×10^{-12} [12]. However, the fact that the decay $K_{\mu e}$ is sensitive to the axial-vector and pseudoscalar (sd) quark transitions, while $K_{\pi\mu e}$ is sensitive to vector, scalar, and tensor transitions, makes these two processes complementary in the search for new phenomena.

This illustrates the significance of the rare decay searches which can be performed at an easily attainable low energy but at the same time can effectively probe the high mass region.

*Now at TRIUMF, Vancouver, BC V6T 2A3
†Now at Rutgers University, Piscataway, NJ 08855
‡Now at Blackmesa Capital, Santa Fe, NM 78712
§Now at Phonak AG, CH-8712 Stäfa, Switzerland
‖Now at Albert-Ludwigs-Universität, D-79104 Freiburg, Germany
¶Now at University of Connecticut, Storrs, CT 06269
**Now at LIGO/Caltech, Pasadena, CA 91125
††Now at SCIPP, University of California, Santa Cruz, CA 95064
‡‡Deceased

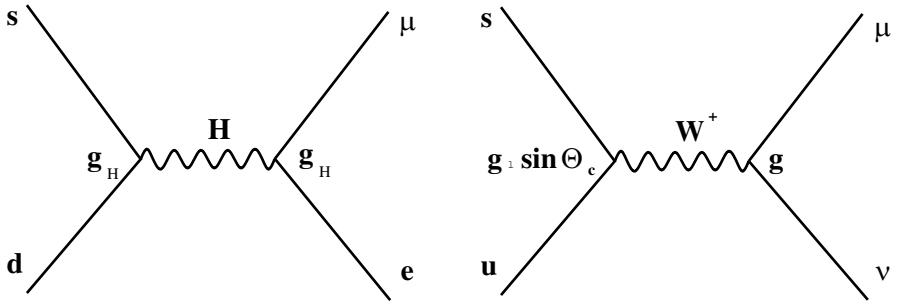

FIG. 1. Left: Feynman diagram for extended technicolor mechanism for $K^+ \to \pi^+ \mu^+ e^-$ decay; right: Feynman diagram for $K^+ \to \pi^0 \mu^+ \nu$ decay. (θ_c is the Cabibbo angle; g_H and g are the ETC and weak coupling constants.)

The analysis outlined here is based on data recorded at the Brookhaven Alternating Gradient Synchrotron (AGS) during a five month run in 1998, employing the E865 detector.

II. EXPERIMENTAL SETUP

A. Overview and design philosophy

To perform a successful search for a rare decay, like the $K_{\pi\mu e}$, two basic conditions must be satisfied: first, the parent particle (K^+) must be produced in copious amounts, and second, the detector must be able to both detect signal and to suppress backgrounds to a level low enough for a signal to be seen. The first condition was met by employing the high intensity proton source (AGS) to create the K^+ beam. With the projected $K_{\pi\mu e}$ single event sensitivity of 10^{-12}, in order to meet the second condition we designed the E865 detector to have excellent event reconstruction and particle identification (PID) capabilities. The particular requirements for the detector's event reconstruction and PID performance were derived from the careful consideration of the possible backgrounds. The dominant way to get a π^+, μ^+, and e^- from a kaon decay is through the decay chain $K^+ \to \pi^+\pi^+\pi^-$ (K_τ), $\pi^+ \to \mu^+\nu$, $\pi^- \to e^-\overline{\nu}$, which has a combined branching ratio of 6.8×10^{-6}. The fact that the in-flight pion decays have to happen within the detector and the neutrinos carry off momentum, distorting an event's kinematics, led to the design of a high-resolution momentum-analyzing spectrometer which allowed charged-particle reconstruction and momentum measurement. The study of the Monte-Carlo simulated events and off-line event reconstruction (to be discussed later) showed that such backgrounds could be suppressed to the level of 10^{-13} by applying simple kinematic cuts. However, the K_τ decay would also mimic the $K_{\pi\mu e}$ if a π^- was misidentified as e^- and π^+ was either misidentified as μ^+ or underwent an in-flight decay ($\pi^+ \to \mu^+\nu$). Another background was caused by rather common kaon decays: $K^+ \to \pi^0\pi^+$ ($K_{\pi 2}$), with a π^+ misidentified as μ^+, and $K^+ \to \pi^0\mu^+\nu$ ($K_{\mu 3}$). Both decays would mimic $K_{\pi\mu e}$ if the π^0 underwent a Dalitz decay ($\pi^0 \to e^+e^-\gamma$) and the e^+ was misidentified as a π^+. In the following we will refer to both decays ($K_{\pi 2}$ and $K_{\mu 3}$ followed by a Dalitz decay of π^0) as $K_{\rm Dal}$. The suppression of the K_τ and $K_{\rm Dal}$ backgrounds required a PID system with abilities to veto π^- (while still being efficient in identifying e^-), veto e^+, and to discriminate μ^+ from π^+.

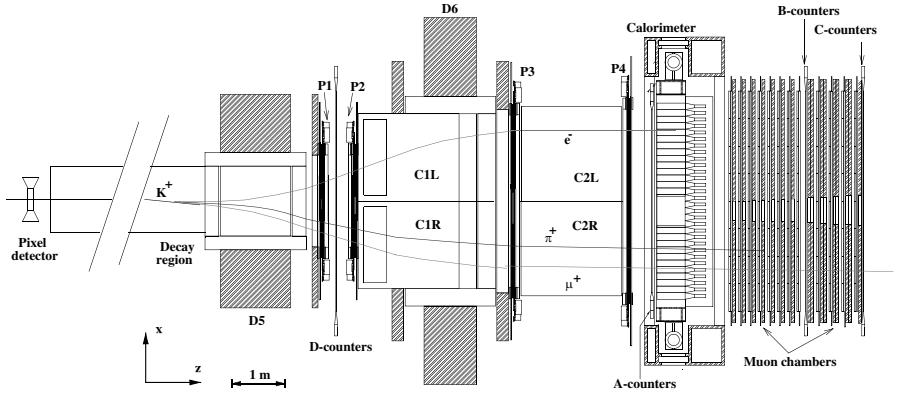

FIG. 2. Overall view of the detector with a simulated $K_{\pi\mu e}$ event (horizontal cross section at beam height). C1, C2: gas Čerenkov counters; P1, P2, P3, P4: proportional chambers; D5, D6: dipole magnets; A, B, C, D: scintillation counter trigger hodoscopes.

A detailed description of the apparatus (see Fig. 2) and the beam arrangement is presented elsewhere [13]. Here we give only a brief overview of the kaon beam and detector elements.

B. Kaon beam

The AGS at Brookhaven National Laboratory served as a source of the primary 25.5 GeV/c proton beam, and delivered about 1×10^{13} protons to the kaon production target in a spill of 2.8 s with a cycle time of 5.1 s. Before the extraction from the AGS, the proton beam was debunched, i.e. particles were distributed over the circumference of the ring to obtain a uniform beam intensity during the spill. The extracted beam of protons, hitting a 15 cm long water-cooled copper target with transverse dimensions 5×5 mm^2, produced a large variety of particles, but mainly pions, protons, and kaons survive. After the production target, the unseparated secondary beam was momentum selected at 6 GeV/c ($\pm 2\%$) and was transported to the beginning of the E865 detector through the specially designed 28 m long A2 beam line [13]. A major concern during the design of the A2 beam line was the muon halo, produced by kaon and pion decays. It was greatly suppressed by tight collimation and two foci followed by dipole magnets, which effectively swept momentum-degraded muons out of the acceptance [13]. During data taking, the beam flux in the A2 beam line was estimated to be 2×10^8 K^+, 4×10^9 π^+, and 2×10^9 protons per spill.

C. Detector overview

The E865 detector was located at the end of the A2 beam line, and its first element was the 5-m long evacuated decay region within which about 6% of the entering kaons decayed. Downstream of the decay region, a dipole magnet (D5) swept the charged decay products away from the beam, with negative particles going mostly to the left, and positive to the right side of the apparatus. The momentum-analyzing spectrometer consisted of proportional wire chambers (PWC), P1-P4, and a second dipole magnet (D6), which steered the particles back into the acceptance region of the detector elements located further downstream. The PWCs, each consisting of four wire planes, were desensitized in the region where the beam passed. This arrangement yielded a momentum resolution of $\sigma_p \approx 0.003\ P^2$ GeV/c, where P, the momentum of the decay products in GeV/c, was typically in the range 0.6 to 3.5 GeV/c.

The first part of the PID system consisted of two large atmospheric-pressure Čerenkov counters (C1 and C2), located upstream and downstream of the P3 wire chamber. Each counter was separated by a thin membrane into two (left and right) parts providing independent particle identification for positive and negative tracks and allowing use of different gases. For the purpose of reducing the possibility of misidentifying a π^- as e^- the left sides (C1L, C2L) were filled with a high Čerenkov threshold gas, hydrogen ($\gamma_t = 60$), and had a light yield of about 2.3 photoelectrons (p.e.) for e^-. To effectively register and veto e^+, the right sides (C1R, C2R) were filled with a low-threshold gas, methane ($\gamma_t = 35$), and had a light yield of about 5.8 p.e. for e^+. In order to reduce beam Čerenkov radiation in C1R and C2R, closed tubes filled with hydrogen gas were placed in the beam region.

The next PID detector element was an electromagnetic calorimeter of the Shashlyk design [14]. It incorporated 582 modules, 11.4 cm by 11.4 cm by 15 radiation lengths each, assembled in a 30×20 array with 18 modules in the middle removed for beam passage. The approximate energy resolution for electrons was $8\%/\sqrt{E(\mathrm{GeV})}$. Typical energy deposition of a minimum ionizing particle was 250 MeV.

The last PID detector element was a muon detection system that was located downstream of the calorimeter and consisted of 24 planes of proportional tubes interspaced by iron plates. The plate thickness was 5 cm between the first eight pairs of planes and 10 cm between the last four. Finally, four arrays of scintillator counter hodoscopes, A, B, C and D, were used for triggering purposes.

D. Trigger requirements

The hardware trigger, described in detail in [13], was designed as a four-level structure with increasing sophistication and response time at each level. The lowest trigger level (T0) selected events with three charged-particle tracks, one on the left and two on the right side, by requiring at least three coincidences between an A-counter slat and the calorimeter module behind it ($\mathrm{A} \cdot \mathrm{SH}$). By using a programmable matrix lookup unit (MLU), for each combination of coincidences between individual counters on the right, only a limited, kinematically acceptable, region on the left was allowed. The MLU was programmed to maximize the acceptance of the three charged body kaon decays by using simulated $K_{\pi\mu e}$ events. In order to reduce contamination from decays occurring downstream of the decay region, at least one coincidence on both left and right sides between the D-counter and $\mathrm{A} \cdot \mathrm{SH}$ was required as well. The T0 signal was ready in about 175 ns after the particle hit the A-counter and had a rate of about 2.5 kHz.

The next trigger level (T1) used information from the Čerenkov counters and the muon range telescope for purpose of PID. In the case of $K_{\pi\mu e}$ the dedicated trigger (MUE) demanded the presence of an electron and a muon. Consequently, the MUE trigger required signals corresponding to at least 0.25 p.e. in both Čerenkov counters on the left side (C1L, C2L) to select e^- and a hit in the muon range telescope (B-hodoscope) to be spatially consistent with the $\mathrm{A} \cdot \mathrm{SH}$ hit in order to select μ^+. The T1 signal was available about 130 ns after the T0, and had a rate of about 1.3 kHz.

The next trigger level (T2) was designed to discriminate between events with high and low e^-e^+ invariant mass. Information from coincident $A \cdot SH$ hits, and Čerenkov counters was used to select events consistent with low vertical separation of e^+e^- tracks (low invariant mass). That trigger was not utilized in the $K_{\pi\mu e}$ search.

The final trigger level (T3) compared the number of hits in each of the PWC planes with a predetermined likelihood distribution obtained off-line. This trigger rejected a small fraction of events that had either too few or too many PWC hits. During data taking, the average rate of T3 was about 1800 per 2.8 s spill or about 0.6 KHz.

In addition to the MUE trigger, several prescaled monitor triggers were recorded, e.g. a minimum bias trigger (TAU), which required only T0 signal and was dominated by the K_τ events, and two triggers sensitive to the $K_{\rm Dal}$ events. The first one (EEPS) demanded the presence of an e^- and e^+ by requiring signals (at least 0.25 p.e.) in both Čerenkov counters on the left and right sides (C1L, C2L, C1R, C2R) and was used for PID studies and background estimates. The second $K_{\rm Dal}$ sensitive trigger (CERENK) was designed to obtain an unbiased response of the Čerenkov counters and required only three out of four sides of the Čerenkov counters (C1L, C2L, C1R, C2R) to have signals above 0.25 p.e.

During a five month data taking period in 1998 we recorded a total of 1.3×10^9 triggers on tape, of which 0.3×10^9 were MUE triggers, successfully reconstructed in the off-line analysis.

III. $K_{\pi\mu e}$ EVENT SELECTION AND OFF-LINE ANALYSIS

A. Event reconstruction

The process of kinematic reconstruction of an event followed the T0 hardware trigger requirements ($A \cdot SH$) and started with the ''clump'' finding, i.e. determining positions of tracks in the calorimeter based on their energy depositions and correlated A-counter hits. For each clump found in the calorimeter, a window in the PWC P4 was defined and space points, requiring at least three of the four wire planes in the chamber, were searched for. Likewise, the space points found in P4 determined windows in P3 and so forth. A track was formed if at least three PWCs contributed with a space point. Next, using the measured magnetic field map inside the dipole magnets, the momentum of each track was fit. For events containing at least three reconstructed tracks, a fitting algorithm was used to determine the decay vertex position by minimizing the quantity S, the root-mean-square (RMS) of the closest approach of the three charged tracks to the common vertex point. For events containing more than three tracks the combination with the smallest S was tagged as the most probable set of track candidates from a kaon decay. Studies of fully reconstructed K_τ events showed that the mean value of S increased for vertices found further upstream (lower z) consistent with Monte-Carlo simulations. The dependence could be fitted with a second-order polynomial [denoted $\bar{S}(z)$]. The normalized quantity $S_{\rm norm} = S/\bar{S}(z)$, which is independent of z, was then used to judge the vertex quality in the $K_{\pi\mu e}$ analysis. As the last step, the information from the PID detectors was assigned to each found track.

B. Event selection

Basic requirements for $K_{\pi\mu e}$ included the presence of a three-charged-track vertex within the decay region of an acceptable quality, $S_{\rm norm}$. In addition, in order to ensure that reconstructed tracks came from a real kaon decay with all the particles being detected, the reconstructed total momentum vector was tracked back to the production target using the first-order beam-line transfer matrix, and its phase space (the kaon momentum P_{K^+}, the position x, y, and the direction θ_x, θ_y) was compared to that of the kaon beam. The five-dimensional phase space of the beam was broken up into three two-dimensional distributions: x versus θ_x, y versus θ_y, and P_{K^+} vs x. The properties of the kaon beam were determined from fully reconstructed K_τ events and were used as input for a corresponding logarithmic likelihood function $L_{\rm target}$ (see Figs. 3 and 9, and also Sec. III D). The invariant mass $M_{\pi\mu e}$, calculated using

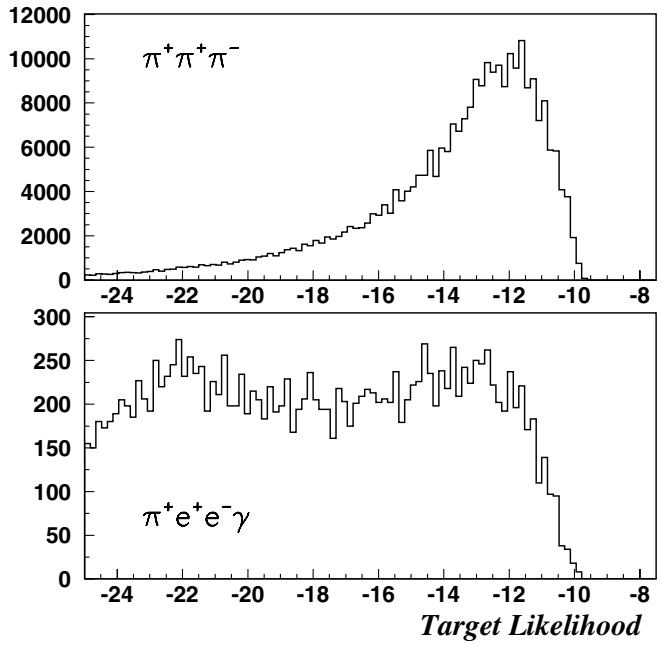

FIG. 3. Target likelihood, $L_{\rm target}$, distributions for the reconstructed $K^+ \to \pi^+\pi^+\pi^-$ (upper) and $K^+ \to \pi^0\pi^+$ with a $\pi^0 \to e^+e^-\gamma$ (lower) events. Poor target likelihood for the $K^+ \to \pi^0\pi^+$ events is caused by the photon, which is not included in the kinematic reconstruction of the kaon momentum vector at the vertex causing it to fall out of the acceptable phase space of the kaon beam. For signal events, $L_{\rm target} > -20$ was required, corresponding to an efficiency of 92%.

TABLE I. Identification efficiencies and probability of misidentification for the primary selection PID cuts. The symbol "→" stands for "identified as."

	$\to \pi^+$	$\to \mu^+$	$\to e^-$
π^+	0.804 ± 0.008	0.066 ± 0.001	$\cdots$
π^-	$\cdots$	$\cdots$	$(8.7 \pm 2.6) \times 10^{-6}$
μ^+	$\cdots$	0.79 ± 0.01	$\cdots$
e^+	$(1.1 \pm 0.1) \times 10^{-5}$	$<(1.1) \times 10^{-5}$	$\cdots$
e^-	$\cdots$	$\cdots$	0.767 ± 0.003

the daughter particle masses (m_π, m_μ, m_e) and their measured momenta, was required to be consistent with the kaon mass, 493.67 MeV, within the resolution, $\sigma_{M_{\pi\mu e}} \approx$ 4 MeV for simulated $K_{\pi\mu e}$ events.

Finally we required an unambiguous identification of e^-, π^+, and μ^+. Electron PID required a signal (at least 0.3 p.e.) in the left sides of both Čerenkov counters (C1L, C2L) with corrected timing within ± 5 ns. In addition, the energy loss in the calorimeter (E) was required to be consistent with the momentum of the track (P), i.e. the ratio E/P to be between 0.65 and 1.5. Pions were identified requiring the absence of a signal above 1.2 p.e. on the right sides of the Čerenkov counters (C2R, C2R) and corresponding corrected timing of more than ± 5 ns. In addition, energy loss in the calorimeter was required to be consistent with that of a minimum ionizing particle or a hadron shower ($E/P < 0.9$). Muons were identified by requiring the absence of a signal above 1.2 p.e. in both Čerenkov counters (C1, C2), energy deposited in the calorimeter consistent with minimum ionization ($E < 450$ MeV), and penetration depth in the muon range consistent with its momentum. Table I summarizes the PID efficiencies and probabilities of misidentification achieved by the above mentioned selection cuts [15].

Although the selection criteria described above provided a high sensitivity for the signal (respective efficiency of each cut was approximately 95%) they let a considerable number of background events pass.

C. Overview of backgrounds

Possible $K_{\pi\mu e}$ backgrounds could be classified into two different types. The first type consisted of rather common kaon decays and was dominated by K_τ and K_{Dal}. These kaon decays could be tagged as $K_{\pi\mu e}$, if kinematic requirements were satisfied and certain daughter particles were either misidentified or underwent an in-flight decay as given in Table II. Because of the excellent particle identification capability of the E865 apparatus, this type of background could be efficiently suppressed by optimizing the PID selection in order to reduce respective misidentification probabilities, $P(\pi^-$ as $e^-)$ and $P(e^+$ as $\pi^+)$. The second type of background consisted of accidental combinations of the π^+, μ^+, and e^- tracks, originating from separate kaon decays, that would satisfy kinematic requirements for $K_{\pi\mu e}$. Such accidental events were usually characterized by uncorrelated track timing and poor kinematic quality (vertex quality S_{norm} and L_{target}). Instead of tightening the selection cuts to suppress these backgrounds, we chose to employ the likelihood method, a brief overview of which is given below.

D. Overview of the likelihood method

In an analysis using cuts, all events that pass the final cuts are considered equally probable to be a signal. The likelihood method, however, allows one to test each event against a particular hypothesis, e.g. the likeliness for a particle to be of a certain type or the decay to be of a particular mode. For example, a pion, passing all the electron PID cuts, would be misidentified as an electron. However, for pions, the values for each of the PID variables will most likely fall at the edge of the various PID distributions while for a real electron they will be in the bulk. Comparing the probabilities of an electron and a pion having a particular PID response allows one to distinguish further between a real and misidentified particle. The same method can be applied to kinematic variables. Thus, the use of a multivariable likelihood function allows one to differentiate quantitatively between signal and background on an event-by-event basis.

The conventional definition of the log-likelihood function is

$$\mathcal{L}(\vec{x}) = \log P(\vec{x}) \tag{2}$$

where $\vec{x} = (x_1, x_2 \ldots x_n)$ is a vector of the measured kinematic and PID response and $P(\vec{x})$ is the n-dimensional probability density function (PDF). In the case where

TABLE II. Main $K^+ \to \pi^+\mu^+e^-$ backgrounds from other K^+ decays.

K^+ decay mode	Misidentification
$K^+ \to \pi^+\pi^+\pi^-$ with $\pi^+ \to \mu^+\nu$, $\pi^- \to e^-\overline{\nu}$	None
$K^+ \to \pi^+\pi^+\pi^-$ with $\pi^+ \to \mu^+\nu$	π^- as e^-
$K^+ \to \pi^+\pi^+\pi^-$ with $\pi^- \to e^-\overline{\nu}$	π^+ as μ^+
$K^+ \to \pi^+\pi^+\pi^-$	π^+ as μ^+ and π^- as e^-
$K^+ \to \pi^+\pi^0$, $\pi^0 \to e^+e^-\gamma$	e^+ as π^+ and π^+ as μ^+
$K^+ \to \pi^+\pi^0$, $\pi^0 \to e^+e^-\gamma$ with $\pi^+ \to \mu^+\nu$	e^+ as π^+
$K^+ \to \pi^0\mu^+\nu$, $\pi^0 \to e^+e^-\gamma$	e^+ as π^+

$x_1, x_2 \ldots x_n$ are independent, the probability can be simplified into

$$P(x_1, x_2, \ldots, x_n) \cong P_1(x_1) \cdot P_2(x_2) \cdot \ldots \cdot P_n(x_n) \qquad (3)$$

where $P_i(x_i)$ is the ith one-dimensional PDF, constructed from the corresponding distribution and x_i is the respective measured response. Using such an approximation, one can rewrite the log likelihood in the following way:

$$\mathcal{L}(\vec{x}) = \sum_{i=1}^{n} \log P_i(x_i). \qquad (4)$$

Generally, an individual PDF can be represented as a continuous analytical function or a binned histogram. While it would be ideal to use the full range of a variable for the likelihood function to maximize the acceptance, it was more practical to use a finite (that would include around 95% of signal events) range, choosing particularly the most sensitive part of the distribution. In most of the cases the range of the likelihood function was defined by the values of the final cuts. The number of bins was selected to be large enough to reflect the shape of a particular distribution. Finally, in constructing a likelihood function, we required each PDF to be normalized to unity.

IV. BACKGROUND STUDIES

A. K_{Dal} background

A large part of the K_{Dal} background was rejected by applying the invariant-mass cut ($M_{ee} > 55$ MeV), since the invariant mass of the e^+e^- pair from the K_{Dal} decays is peaked at low values (see Fig. 4). Events containing photons registered in the calorimeter with a corrected timing within ± 2 ns were rejected. Additional rejection was achieved by the target likelihood cut since, due to the presence of the photon that was not included in the kinematic reconstruction, the total kaon momentum vector was usually inconsistent with that of the kaon beam. To estimate the level of the K_{Dal} background we used the EEPS triggered data. We selected $e^+\mu^+e^-$ events that could mimic $K_{\pi\mu e}$ (if an e^+ was misidentified as a π^+) by applying the $K_{\pi\mu e}$ kinematic selection cuts and requiring identification of the μ^+ and e^-. Events, that were selected that way, were scaled by the EEPS trigger hardware prescale factor (20) and a corresponding misidentification probability—$P(e^+$ as $\pi^+)$. To reduce the misidentification probability we constructed the log-likelihood function for the purpose of π^+ identification. The likelihood included the ratio E/P and the quantity E_{ratio} describing the spatial spread of the electromagnetic shower in the calorimeter. The latter variable is defined as the ratio of the energy deposited in the central module, i.e. the module to which a track points, to the total energy, which also includes the three most adjacent modules [15].

The selected cut value for the π^+ PID likelihood, which resulted in the estimated misidentification probability $P(e^+$ as $\pi^+) = (2.5 \pm 0.3) \times 10^{-6}$, ensured a satisfactory suppression of the estimated K_{Dal} background to the level of 0.09 ± 0.01 events.

B. K_τ background

Kinematically, the K_τ background was suppressed by applying the invariant $M_{\pi\mu e}$ mass cut, since assigning lower masses (m_e, m_μ) to the pions from the K_τ decay effectively removed mass from the system (see Fig. 4). To estimate the level of the K_τ background we used the TAU triggered data. We selected $\pi^+\mu^+\pi^-$ events that could mimic $K_{\pi\mu e}$ (if a π^- was misidentified as an e^-) by applying the $K_{\pi\mu e}$ kinematic selection cuts and requiring identification of the π^+ and μ^+. Events that were selected this way were scaled by the TAU trigger hardware prescale factor (10^4) and a corresponding misidentification probability—$P(\pi^-$ as $e^-)$. To reduce the misidentification probability we constructed the log-likelihood function for the purpose of e^- identification. The likelihood included

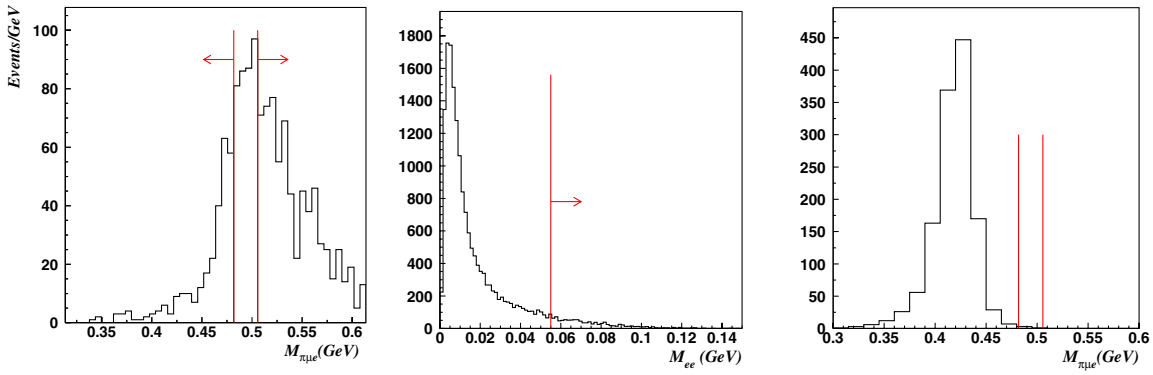

FIG. 4 (color online). Left: $M_{\pi\mu e}$ mass distribution for $e^+\mu^+e^-$ events measured with the EEPS monitor trigger (K_{Dal} background). Vertical lines mark the $M_{\pi\mu e}$ mass signal region; center: M_{ee} invariant-mass spectrum for measured K_{Dal} events. The cut on $M_{ee} > 0.055$ GeV removes 94% of the K_{Dal} events; right: $M_{\pi\mu e}$ mass spectrum for the $\pi^+\mu^+\pi^-$ events measured with the TAU monitor trigger (K_τ background). Vertical lines mark the $M_{\pi\mu e}$ mass signal region.

the number of p.e. and time registered by C1L and C2L, the ratio E/P in the calorimeter, and again the variable $E_{\rm ratio}$. The selected cut value for the e^- PID likelihood, which resulted in the estimated misidentification probability $P(\pi^- \text{ as } e^-) = (2.4 \pm 1.4) \times 10^{-6}$, ensured a satisfactory suppression of the estimated K_τ background to the level of 0.1 ± 0.1 events.

C. Accidental background

To reject accidental events effectively it was crucial to study and understand the precise accidental event mechanisms. The simplest mechanism would be a combination of two tracks from a real kaon decay and a single track from another decay, or beam background *(2+1)*. Another possibility is that all three tracks would originate from different decays or beam background *(1+1+1)*. To determine what particular combinations of accidental tracks were dominant, the time structure of accidental events was examined. The time of each track (t_e, t_π, t_μ) was defined as the average of the times registered by the A-counter and the calorimeter. The $t_e - t_\pi$ and $t_e - t_\mu$ track time differences were chosen to describe the event timing. A control sample of accidental three-track events was selected by requiring the reconstructed kaon momentum to be greater than that of the beam ($P > 7$ GeV/c) and removing the $L_{\rm target}$ cut. To increase the sample size, cuts on the vertex quality $S_{\rm norm}$, and the invariant mass $M_{\pi\mu e}$, were removed. Accidental events, selected in such a manner, showed a distinct *cross* in the scatter plot of the track time difference as seen in Fig. 5(a), indicating that accidental events had two main components. The horizontal part of the cross identified the π^+ as the additional accidental track paired with the two tracks ($e^-\mu^+$) from another decay and the vertical part identified μ^+ as an accidental track. Accidental e^- tracks were not observed, since the scatter plot did not show a linear correlation between the variables. Finally, triple coincidences *(1+1+1)* appeared uniformly scattered and as we expected their contribution was negligible. For the signal events, the correlation between the track time difference was examined using the measured response of the reconstructed K_τ events as can be seen in Fig. 5(b).

The difference in the time response between the signal and accidental events was used to create a time quality estimator variable, $T_{\rm max}$, which was defined as the maximum absolute difference between the track times t_π or t_μ and the average times of the two remaining tracks $t_{e\mu}$ or $t_{e\pi}$, respectively. The ratio between the two accidental components was estimated to be approximately one to two (34% $e\mu + \pi$ and 66% $e\pi + \mu$). The most reasonable candidate for the two-track part ($e\pi$) of the main accidental component ($e\pi + \mu$) was the $K_{\pi 2}$ decay with a subsequent $\pi^0 \to e^+e^-\gamma$ decay. In the two-body decay $K_{\pi 2}$ the pion momentum and angle of the pion track at the vertex are correlated, as shown in Fig. 5(c). On the other hand, three-body decay signal events do not show such a correlation [Fig. 5(d)]. The effect was best observed when the π^+ angle-momentum dependence was projected on the axis orthogonal to the axis of almost linear correlation between the angle and momentum of a π^+ from the $K_{\pi 2}$ decay as shown in Fig. 5(c), equivalent to using the variable $z = \theta_\pi/0.14 + P_\pi/5$ (P_π in GeV/c and θ in radians). By requiring the variable z to be less than one, 60% of accidental background events were rejected with 80% of them being from the $e\pi + \mu$ component. This caused only a 13.5% loss in signal sensitivity.

The number of accidental background events was estimated using the number of observed out-of-time $K_{\pi\mu e}$ candidates ($3 \text{ ns} < T_{\rm max} < 8$ ns) which otherwise satisfied all $K_{\pi\mu e}$ cuts. To extrapolate into the acceptable in-time signal region, the timing distribution of the high momentum ($P > 6.9$ GeV/c) $K_{\pi\mu e}$ candidates was used. From that timing distribution we determined the projection factor R (the ratio between the number of high momentum $K_{\pi\mu e}$ candidates with $T_{\rm max} < 3$ ns and the ones with the $T_{\rm max}$ in the range of 3 to 8 ns). The expected level of accidental background in the signal region was thus determined to be 8.2 ± 1.9 events. Data study confirmed that the projection factor R, used for accidental background estimate, did not depend on the momentum cutoff value, which was varied

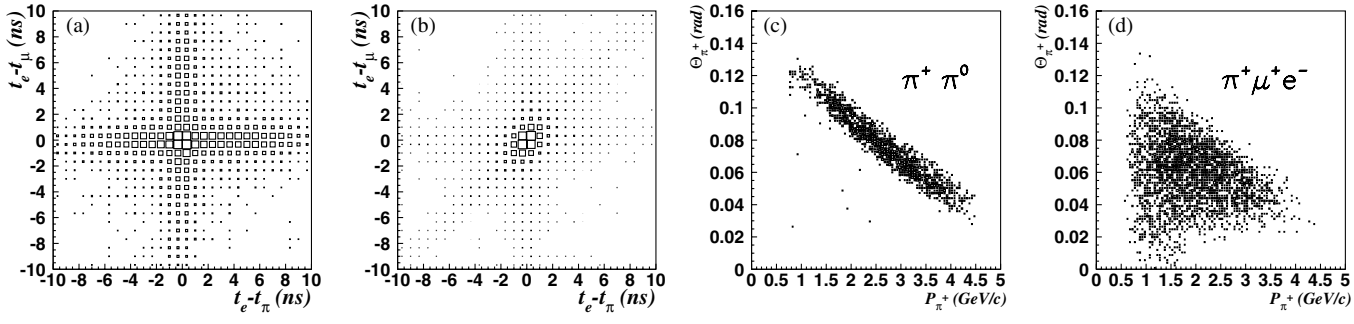

FIG. 5. Scatter plot of differences between track times: $t_{\pi^-(1)} - t_{\pi^+(2)}$ versus $t_{\pi^-(1)} - t_{\pi^+(3)}$ for the high momentum accidental events [(a)] and measured K_τ events [(b)]; scatter plot of π^+ track angle at the vertex (θ) versus π^+ momentum (P_π) for the simulated $K^+ \to \pi^0\pi^+$ [(c)] and $K^+ \to \pi^+\mu^+e^-$ [(d)] events.

in the range of 6.9 to 7.7 GeV/c. To test the validity of using high momentum accidentals to extract the time distribution of $K_{\pi\mu e}$ accidental background, we selected a sample of $K_{\pi\mu e}$ candidates with the $M_{\pi\mu e}$ mass cut reversed and no timing ($T_{\max}$) cut applied. The timing response from the latter sample was a superposition of the timing response from $K_{\pi\mu e}$ accidental background and the timing response of the K_τ and K_{Dal} backgrounds. The tail ($T_{\max} > 3$ ns) of the timing spectrum, which was dominated by accidental events in that sample, matched the timing distribution of the high momentum events.

V. LIKELIHOOD ANALYSIS

A. Check of the background estimates

Following the principles of the so-called *blind analysis* the $K_{\pi\mu e}$ candidate events were examined, while the signal region was excluded by reversing the cut on the invariant kaon mass ($|M_{\pi\mu e} - 0.4937| > 0.012$ GeV). The invariant $M_{\pi\mu e}$ mass distribution for the 216 observed $K_{\pi\mu e}$ candidates as illustrated in Fig. 6(d) exhibited a peak at lower mass values, which was caused by the K_τ background. In order to check the validity of the background estimates, the $M_{\pi\mu e}$ mass distribution for the $K_{\pi\mu e}$ candidates was compared with that of the predicted backgrounds. Following the same algorithm as that of the background estimates the $M_{\pi\mu e}$ distributions were generated for the main background processes using measured data: for the K_τ background, observed $\pi^-\pi^+\mu^+$ events were scaled by the misidentification probability $P(\pi^-$ as $e^-)$. For the K_{Dal} background, observed $e^-e^+\mu^+$ events were scaled by the misidentification probability $P(e^+$ as $\pi^+)$. Finally, for the accidental background, the out-of-time $K_{\pi\mu e}$ candidate events were scaled by the projection factor R (ratio of in-time to out-of-time accidental events). The satisfactory agreement between the predicted and observed events as displayed in Fig. 6(d) served as a consistency check for our estimates of the background processes and misidentification probabilities [$P(e^+$ as $\pi^+)$ and $P(\pi^-$ as $e^-)$].

B. General $K_{\pi\mu e}$ likelihood

The background study indicated that 98% of the background to $K_{\pi\mu e}$ was due to accidental events. As discussed above, rather than imposing additional or tighter cuts, the likelihood function was chosen to suppress this background. The general $K_{\pi\mu e}$ likelihood was constructed using the kinematic and timing variables which showed the most difference in their response for signal and accidental events. The following six variables were selected: target likelihood L_{target}, vertex quality S_{norm}, reconstructed $M_{\pi\mu e}$ mass, timing cut $T_{\max}$, sum of the χ^2 for the track reconstruction fits, and T_{extra}, the minimum time difference between the time of the extra clump in the calorimeter and time of the track pair, which is closest in time. Data studies showed that within the statistical uncertainties the variables chosen were uncorrelated both for the signal and for the background. This allowed us to calculate the general likelihood for $K_{\pi\mu e}$ and accidentals in the following manner:

$$\mathcal{L}_{\pi\mu e}(x_1 \ldots x_6) = \sum_{i=1}^{6} \log P_i^{\pi\mu e}(x_i), \tag{5}$$

$$\mathcal{L}_{\mathrm{Acc}}(x_1 \ldots x_6) = \sum_{i=1}^{6} \log P_i^{\mathrm{Acc}}(x_i), \tag{6}$$

where $x_i = (L_{\mathrm{target}}, S_{\mathrm{norm}}, M_{\pi\mu e}, \chi^2_{\mathrm{Track}}, T_{\max}, T_{\mathrm{extra}})$ and $P_i^{\pi\mu e}$, P_i^{Acc} are one-dimensional PDFs for signal and background, respectively. For the signal, only the $M_{\pi\mu e}$ mass PDF was generated from the Monte-Carlo simulated events with remaining PDFs generated from the measured data by using reconstructed K_τ events. For the accidental events, respective PDFs were generated from the data, using out-of-time $K_{\pi\mu e}$ candidates, except for $T_{\max}$ and T_{extra} for which the PDFs were generated using high momentum $K_{\pi\mu e}$ candidates [15]. The total relative likelihood $\mathcal{L}$ for $K_{\pi\mu e}$ was defined as the difference between $\mathcal{L}_{\pi\mu e}(x_1 \ldots x_6)$ and $\mathcal{L}_{\mathrm{Acc}}(x_1 \ldots x_6)$.

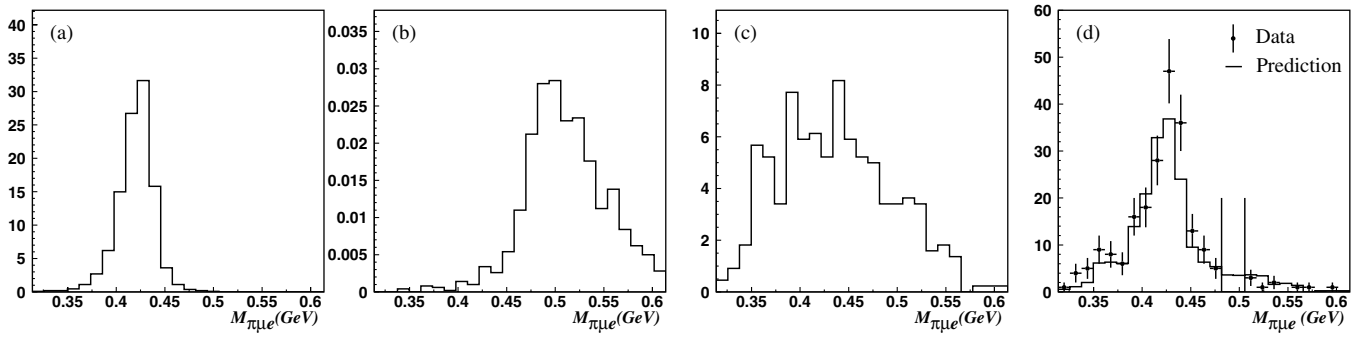

FIG. 6. The reconstructed $M_{\pi\mu e}$ mass distribution for the (a) estimated K_τ background; (b) estimated K_{Dal} background; (c) estimated accidental background. (d) Comparison of the $M_{\pi\mu e}$ mass distribution for the $K_{\pi\mu e}$ data (markers with error bars) and total estimated background (histogram).

The likelihood distribution for signal events was generated using the measured data. With the exception of the invariant $M_{\pi\mu e}$ mass, the response of the K_τ events for the likelihood variables was identical to that of the signal. The $M_{\pi\pi\pi}$ mass resolution of K_τ events had to be scaled by a factor of 1.725 in order to match the mass resolution of $K_{\pi\mu e}$ events. The latter was determined from the Monte-Carlo simulations [15]. Consequently, the signal likelihood template was generated using the good K_τ events with the scaled $M_{\pi\pi\pi}$ mass used as the $M_{\pi\mu e}$ mass.

The likelihood distribution for accidental events was obtained using a sample of out-of-time $K_{\pi\mu e}$ candidate events. Since all six variables used in the likelihood had to be within the final cut values, the timing response was generated from a library of the measured timing response of the high momentum ($P > 7$ GeV/c) accidental events [15]. To test the assumption about the independence of the variables used in the general likelihood, their response was simulated directly from the corresponding PDFs. The fact that the simulated likelihood distributions compared favorably with the ones derived from the data (see Fig. 7) confirmed our study of variables correlation and ensured the validity of the likelihood factorization of Eq. (3).

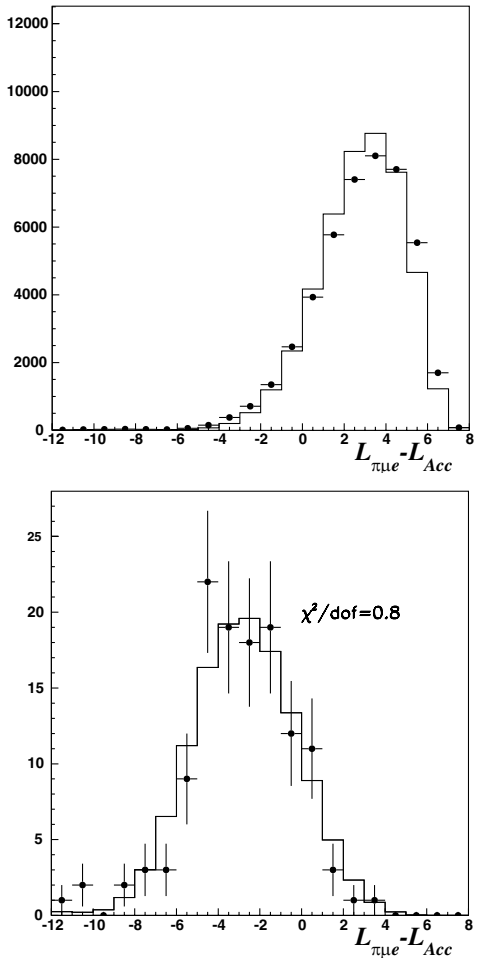

FIG. 7. Comparison of the general likelihood distributions for measured (markers with error bars) and simulated directly from the PDF events for the $K_{\pi\mu e}$ (top) and the accidental background (bottom). The $K_{\pi\mu e}$ likelihood was calculated from the measured K_τ event sample (see text for details).

C. Determining the number of $K_{\pi\mu e}$ events

1. The Bayesian approach

To determine the number of signal events, in the presence of a significant number of accidental background events (8.2 ± 1.9), the Bayesian approach [16] was used. The likelihood function for Poisson-distributed data was defined as follows:

$$L_P(\vec{m};\vec{n}) = \prod_{i=1}^{k} \frac{m_i^{n_i} e^{-m_i}}{n_i!} \tag{7}$$

where

k = arbitrarily chosen number of bins,

n_i = the number of observed events in the ith bin,

$\vec{n} = (n_1, n_2, \ldots, n_k)$,

N = total number of observed events $\left(= \sum_{i=1}^{k} n_i\right)$,

m_i = the number of expected events in the ith bin,

$\vec{m} = (m_1, m_2, \ldots, m_k)$.

The number of expected events in the ith bin of the likelihood distribution was parametrized in the following

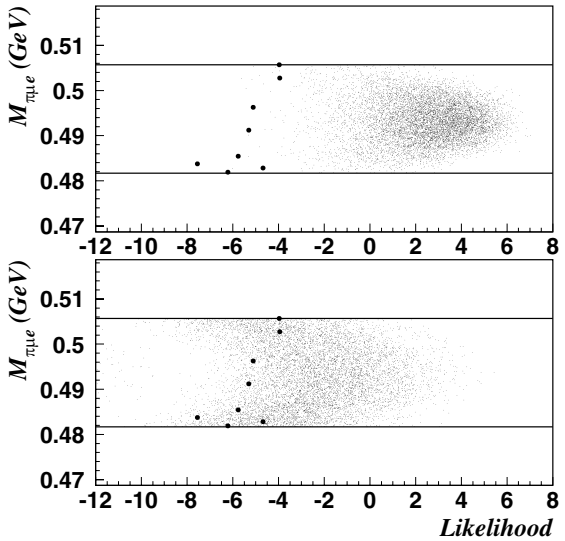

FIG. 8. Scatter plot of $K_{\pi\mu e}$ data (bold dots) and simulated signal (top) and background (bottom). The abscissa is the log likelihood of the reconstructed events; the ordinate is the invariant mass ($M_{\pi\mu e}$) of the detected particles. The horizontal lines mark the 3σ mass region.

way:

$$m_i = N_{\rm sig} P_{\pi\mu e_i} + N_{\rm bg} P_{{\rm Acc}_i} \tag{8}$$

where $N_{\rm sig}$ was the number of $K_{\pi\mu e}$ events, $N_{\rm bg}$ was the number of accidental events, and $P_{\pi\mu e_i}$ and $P_{{\rm Acc}_i}$ were the probabilities to be in the ith bin for the signal and the accidental background, respectively. The parameter $N_{\rm bg}$ was determined earlier from the study of accidental background. The probabilities ($P_{\pi\mu e_i}$ and $P_{{\rm Acc}_i}$) were extracted using the likelihood templates, created for the $K_{\pi\mu e}$ and accidental hypothesis. The statistical uncertainty of the background estimate was accounted for by adding a Gaussian factor to Eq. (7):

$$L_P = \prod_{i=1}^{k} \frac{m_i^{n_i} e^{-m_i}}{n_i!} \times \exp\left(-\frac{(N_{\rm bg} - N_{\rm bg}^{(0)})^2}{2\sigma_{\rm bg}^2}\right) \tag{9}$$

where

$$N_{\rm bg}^{(0)} = 8.2 \quad \text{and} \quad \sigma_{\rm bg} = 1.9.$$

Under the parametrization of m_i, given in Eq. (8), the Poisson-distributed data likelihood function, Eq. (9), was transformed: $L_P(\vec{m};\vec{n}) \Rightarrow L(N_{\rm sig}, N_{\rm bg})$. As the next step, the probability was normalized to unity:

$$P(N_{\rm sig}, N_{\rm bg}) = \frac{L(N_{\rm sig}, N_{\rm bg})}{\int_0^\infty dN_{\rm bg} \int_0^\infty L(N_{\rm sig}, N_{\rm bg}) dN_{\rm sig}}. \tag{10}$$

To determine the upper limit on the number of signal events at the 90% C.L. one integrates the probability $P(N_{\rm sig}, N_{\rm bg})$ from zero up to $N_{\rm sig}^{\rm max}$, until the 0.9 probability level is reached:

$$\frac{\int_0^\infty dN_{\rm bg} \int_0^{N_{\rm sig}^{\rm max}} L(N_{\rm sig}, N_{\rm bg}) dN_{\rm sig}}{\int_0^\infty dN_{\rm bg} \int_0^\infty L(N_{\rm sig}, N_{\rm bg}) dN_{\rm sig}} = 0.90. \tag{11}$$

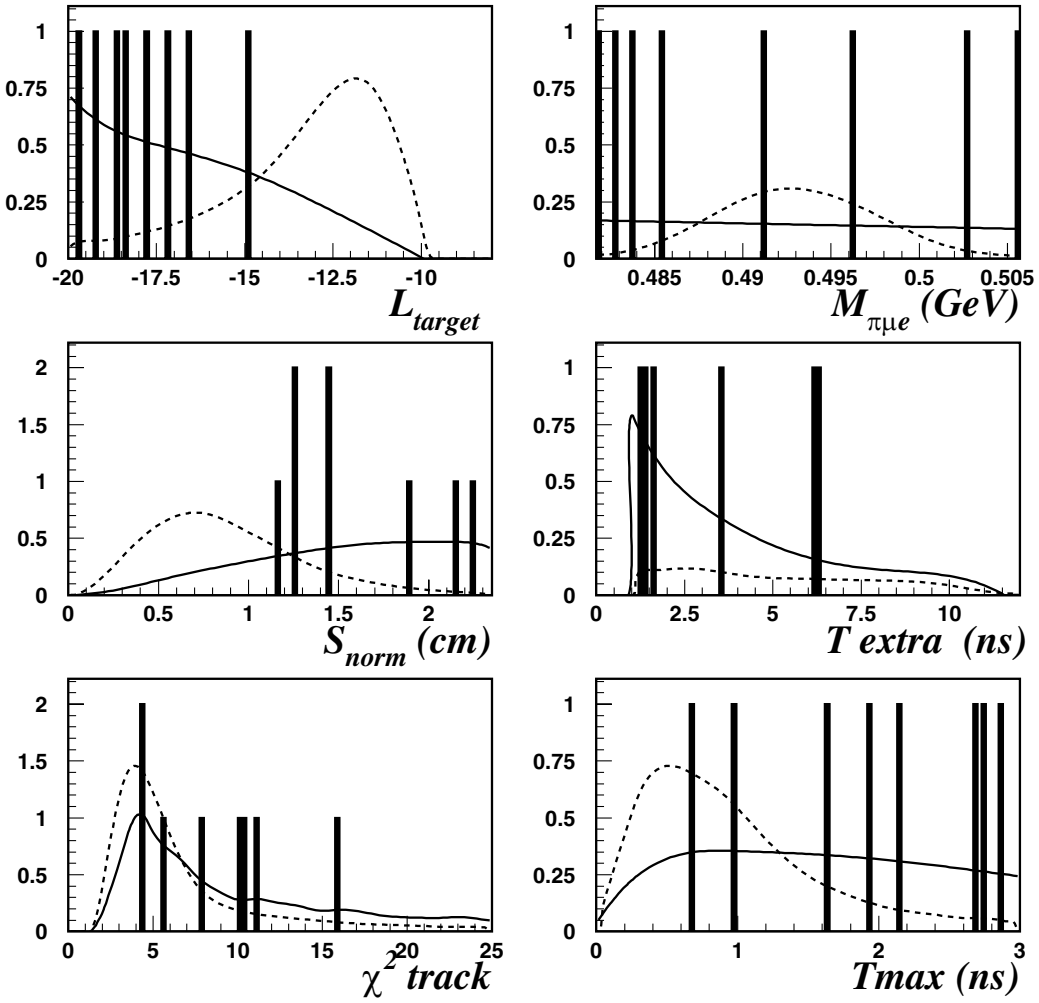

FIG. 9. Distributions of target likelihood ($L_{\rm target}$), reconstructed kaon mass $M_{\pi\mu e}$, vertex quality $S_{\rm norm}$, minimum time difference between extra clumps in the calorimeter and closest in-time track pair ($T_{\rm extra}$), sum of track's χ^2, and $T_{\rm max}$ for the $K_{\pi\mu e}$ data. For reference purposes, corresponding PDFs are shown for signal (dotted line) and background (solid line) hypotheses.

By solving Eq. (11) one can numerically determine the number of signal events at the 90% C.L.

2. Signal region

Eight events survived the final $K_{\pi\mu e}$ selection, which was consistent with our background prediction of 8.2 ± 1.9. Examination of the likelihood distribution of the surviving events demonstrates that they are clearly not consistent with the signal hypothesis (see Fig. 8). By solving Eq. (11) for the surviving events an upper limit on the number of $K_{\pi\mu e}$ events at a 90% C.L. was determined to be $N_{\rm sig} < 2.4$.

A simple cut on the likelihood would remove all surviving events with only a 3% loss in efficiency.

The distributions of the six variables used in the general likelihood for the observed eight events along with the respective signal and background PDFs are presented in Fig. 9.

VI. NORMALIZATION AND ACCEPTANCE CALCULATION

To calculate the $K_{\pi\mu e}$ branching ratio, the total number of K^+ decays had to be determined. The total number of K^+ decays can be determined indirectly by normalization to a decay mode that is well understood and observable in the detector, and has a relatively high branching ratio. We used the K_τ decay as the normalization mode. The upper limit on the branching ratio was determined according to the following formula:

$$B(\pi\mu e) < B(\pi\pi\pi) \cdot \frac{N(\pi\mu e)}{N(\pi\pi\pi)} \cdot \frac{\mathrm{Accep}(\pi\pi\pi)}{\mathrm{Accep}(\pi\mu e)} \cdot C \quad (12)$$

where B denotes the branching ratio of the decay, $N(\pi\mu e)$ is the 90% C.L. upper limit on the number of signal events, $N(\pi\pi\pi)$ is the number of observed K_τ events, adjusted for prescale factors, Accep is acceptance of the detector system, and finally C is the correction factor accounting for efficiency differences between the selection of signal ($K_{\pi\mu e}$) and normalizer (K_τ) decay modes (see Sec. VI C).

A. Total number of K_τ events

As mentioned in Sec. II D, we collected K_τ decays in a minimum bias TAU trigger concurrently with $K_{\pi\mu e}$ events. This allowed us to deduce the number of normalization K_τ events by analyzing the TAU triggered data. To reduce the systematic uncertainties in the acceptance ratio calculation, the normalization sample was kinematically selected using cuts which were identical to the ones for $K_{\pi\mu e}$. However, some of the cuts used for the $K_{\pi\mu e}$ selection, including the PID cuts, the invariant M_{ee} mass cut, and a cut ($z < 1$) that rejected π^+'s originating from $K_{\pi 2}$ decays, were not applied.

The application of the selection cuts (see Table III) yielded 77 226 events. The total number of the K_τ events was determined after accounting for the hardware (10^4) and software (50) prescale factors:

$$N(\pi\pi\pi) = 77226 \times 50 \times 10^4 = 3.86 \times 10^{10} \text{ events.} \quad (13)$$

B. Monte-Carlo simulations

The simulation started with the kaon beam at the upstream end of the decay region. The phase space of the beam was deduced from a large sample of K_τ events, for which the incident K^+ could be fully reconstructed. The K^+ was then allowed to decay in a preselected mode along its trajectory in the decay region. The interactions of the beam particles and the decay products with the detector were simulated using the GEANT3 [17] software package from CERN. The simulated detector response was then analyzed using the same reconstruction and selection procedures as data events.

In order to check the quality of the simulation, control distributions for various kinematic variables were compared to measured data for K_τ and $K_{\rm Dal}$ decays. Because of the different phase space and different daughter particles, those two decays have significantly different control distributions. The quality of the simulation is demonstrated in Fig. 10, which displays the vertex quality $S_{\rm norm}$, which is a crucial parameter for event reconstruction; the position of

TABLE III. Cuts used for determining the number of K_τ decays.

Variable	Description	Efficiency
$S_{\rm norm}$	vertex quality	0.927 ± 0.005
$\sum_{i=1}^{3} \chi^2_{\rm trk_i}$	sum of track's fit χ^2	0.967 ± 0.005
$L_{\rm target}$	target likelihood	0.923 ± 0.005
$T_{\rm max}$	time quality indicator	0.911 ± 0.004
$T_{\rm extra}$	no extra clumps in the calorimeter within 1 ns	0.956 ± 0.005
N_γ	photons veto	0.965 ± 0.005
$S_{\rm 2trk}$	two-track vertex quality	0.959 ± 0.005
$M_{\pi\pi\pi}$	reconstructed kaon mass	0.976 ± 0.005

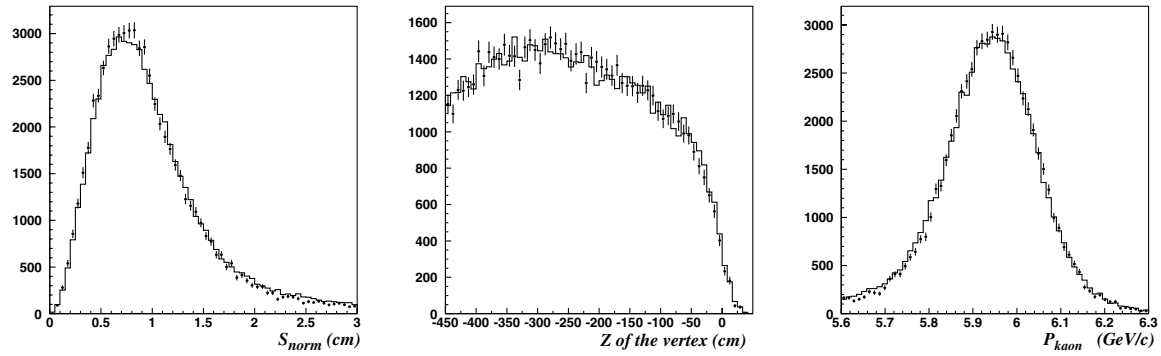

FIG. 10. Comparison of the Monte Carlo simulations of K_τ decays (histogram) with data (markers with error bars). Left: distance of closest approach $S_{\rm norm}$ to the common vertex for the three charged tracks; center: distribution of decay vertices along the beam direction Z ($Z = 0$ at the entrance of the first dipole magnet); right: reconstructed K^+ momentum.

the vertex along the direction of the beam, Z of the vertex, which depends on the detector acceptance; and reconstructed kaon momentum $P_{\rm kaon}$, which is sensitive to the resolution.

As an additional consistency check, we estimated the number of observed K_τ decays, as registered by the TAU trigger, from the number of observed low M_{ee} mass $K_{\rm Dal}$ events, as registered by the EEPS trigger, by applying the acceptance ratio obtained from the Monte-Carlo simulations. For the calculation of the low M_{ee} mass $K_{\rm Dal}$ events acceptance, we simulated $K^+ \to \pi^0\pi^+$, $K^+ \to \pi^0\mu^+\nu$, $K^+ \to \pi^0 e^+\nu$, $K^+ \to \pi^+\pi^0\pi^0$ decays (all with a subsequent decay of a $\pi^0 \to e^+e^-\gamma$) and weighted them by their measured branching ratios [16]. The predicted number of K_τ decays was consistent within the statistical uncertainty (1.5%) with the number of observed K_τ events [15]. This underlined our understanding of the geometrical acceptance and the efficiency of the various detector elements.

For 2.5×10^5 simulated K_τ events 31 600 were accepted, resulting in

$$\text{Accep}\,(\pi\pi\pi) = 0.1264 \pm 0.0008. \tag{14}$$

For 2.5×10^5 simulated $K_{\pi\mu e}$ events 17 003 were accepted, resulting in

$$\text{Accep}\,(\pi\mu e) = 0.0680 \pm 0.0005 \tag{15}$$

and

$$\frac{\text{Accep}(\pi\pi\pi)}{\text{Accep}(\pi\mu e)} = 1.86 \pm 0.02. \tag{16}$$

To estimate the influence of alignment inaccuracies we varied the size of a dead (desensitized) region where the beam passed (see Sec. II C), which was the most sensitive parameter for both $K_{\pi\mu e}$ and K_τ decays acceptance. We considered three cases, for which we defined a smaller ($\Delta x = \Delta y = -0.5$ cm), nominal, and a larger dead region ($\Delta x = \Delta y = +0.5$ cm). While the changes in the acceptance of the K_τ and $K_{\pi\mu e}$ decays were noticeable, the acceptance ratio showed the following variation:

(i) 1.88 ± 0.02—smaller dead region;
(ii) 1.86 ± 0.02—nominal dead region;
(iii) 1.83 ± 0.02—larger dead region.

From this study we deduced a systematic uncertainty of roughly 1.5% on the acceptance ratio:

$$\frac{\text{Accep}(\pi\pi\pi)}{\text{Accep}(\pi\mu e)} = 1.86 \pm 0.02(\text{stat.}) \pm 0.03(\text{syst.}). \tag{17}$$

C. Correction factors

The correction factor C in Eq. (12) contains efficiencies to account for the difference in reconstructing K_τ and $K_{\pi\mu e}$ events. As described in Sec. VI A, most of the kinematic cuts for the K_τ sample selection were also applied to select

TABLE IV. Efficiencies used to calculate correction factor.

Efficiencies	Description	Value
ϵ_π	π^+ detection	0.781 ± 0.004
ϵ_μ	μ^+ detection	0.79 ± 0.01
ϵ_e	e^- detection	0.745 ± 0.003
$\epsilon_{M_{ee}}$	invariant-mass cut $M_{e^-\pi^+} > 55$ MeV and $M_{e^-\mu^+} > 55$ MeV	0.919 ± 0.007
ϵ_{CL}	e^- required on the left side of the Čerenkov counters	0.926 ± 0.008
ϵ_{CR}	π^+ required on the right side of the Čerenkov counters	0.891 ± 0.008
ϵ_z	reject π^+ from $K^+ \to \pi^0\pi^+$ decay	0.865 ± 0.009

$K_{\pi\mu e}$ events and the corresponding efficiencies were the same for both decay modes. The correction factor was calculated, as a reciprocal of the product of the selection cut efficiencies specific to the $K_{\pi\mu e}$ (see Table IV), to be $C = 3.32 \pm 0.08$. The bulk of C, 2.17, is the reciprocal of the product of the π^+, μ^+, and e^- PID efficiencies, while the remaining factor of 1.53 results from the specific $K_{\pi\mu e}$ kinematic cuts.

VII. RESULTS AND CONCLUSIONS

With the $B(\pi\pi\pi) = 5.58 \pm 0.03\%$ [16], and all the other factors in Eq. (12) determined, the upper limit on the $K_{\pi\mu e}$ branching ratio is set at

$$B(K^+ \to \pi^+\mu^+e^-) < 2.1 \times 10^{-11} \quad (90\% \text{ C.L.}). \quad (18)$$

The details of the analysis of the final data set obtained by E865 are described in this paper. Here, we summarize the search for the decay $K^+ \to \pi^+\mu^+e^-$ at BNL, which included a series of four measurements in which the following 90% C.L. upper limits were obtained: 2.1×10^{-10} [8], 2.0×10^{-10} [9], 3.9×10^{-11} [10,11], and 2.1×10^{-11} (this paper). Since the last two measurements were not background free, we analyzed the combined likelihood function constructed as the product of the likelihood functions for the separate measurements to establish a combined upper limit. For the final data set, this function is described above in Eq. (9). The analogous function, based on the distributions shown in Fig. 4 of Ref. [11], was used for the 1996 data. The only common parameter was a $K^+ \to \pi^+\mu^+e^-$ branching ratio B, introduced into the likelihood function via

$$N_{\text{sig}} = N_K^{\text{eff}} B,$$

where N_K^{eff} was the effective (corrected for $K_{\pi\mu e}$ acceptance) number of kaon decays in a given experimental run. For the background and signal free measurements of Refs. [8] (E777) and [9], the likelihood function [Eq. (9)] is reduced to the simple form $\exp(-N_K^{\text{eff}} B)$.

Using the Bayesian approach in the analysis of the combined likelihood function, we have obtained

$$B(K+ \to \pi^+\mu^+e^-) < 1.3 \times 10^{-11} \quad (90\% \text{ C.L.}).$$

Although no evidence of new physics was found, the parameter space of the existing extension theories that allow LFNV was reduced. Particularly, as discussed in Sec. I, the mass, M_H, of the corresponding extended technicolor boson, with strength equal to that of the weak interaction, is bound by the limit obtained on the $K_{\pi\mu e}$ branching ratio to be greater than ≈ 80 TeV.

ACKNOWLEDGMENTS

We gratefully acknowledge the contributions to the success of this experiment by Dave Phillips, the staff and management of the AGS at the Brookhaven National Laboratory, and the technical staffs of the participating institutions. Also, we would like to acknowledge discussions concerning this analysis with Dr. Andries van der Schaaf (Zurich) and contributions to earlier stages of the experiment by Dr. Peter Robman (Zurich). This work was supported in part by the U. S. Department of Energy, the National Science Foundations of the USA, Russia and Switzerland, and the Research Corporation.

[1] A. B. McDonald *et al.* (SNO Collaboration), AIP Conf. Proc. **646**, 43 (2003).
[2] P. Langacker, S. U. Sankar, and K. Schilcher, Phys. Rev. D **38**, 2841 (1988).
[3] R. N. Cahn and H. Harari, Nucl. Phys. **B176**, 135 (1980).
[4] O. Shanker, Nucl. Phys. **B185**, 382 (1981).
[5] E. Farhi and L. Susskind, Phys. Rep. **74**, 277 (1981).
[6] H. E. Haber and G. L. Kane, Phys. Rep. **117**, 75 (1985).
[7] A. M. Diamant-Berger *et al.*, Phys. Lett. B **62**, 485 (1976).
[8] A. M. Lee *et al.*, Phys. Rev. Lett. **64**, 165 (1990).
[9] D. R. Bergman, Ph.D. thesis, Yale University, 1997; S. Pislak, Ph.D. thesis, University of Zürich, 1997; the results were quoted in Ref. [11]. Available at http://www.phy.bnl.gov/~hma/e865/thesis.html.
[10] H. Do, Ph.D. thesis, Yale University, 2000.
[11] R. Appel *et al.*, Phys. Rev. Lett. **85**, 2450 (2000).
[12] D. Ambrose *et al.*, Phys. Rev. Lett. **81**, 5734 (1998).
[13] R. Appel *et al.*, Nucl. Instrum. Methods Phys. Res., Sect. A **479**, 349 (2002).
[14] G. S. Atoyan *et al.*, Nucl. Instrum. Methods Phys. Res., Sect. A **320**, 144 (1992).
[15] A. Sher, Ph.D. thesis, University of Zürich, 2004.
[16] S. Eidelman *et al.* (Particle Data Group), Phys. Lett. B **592**, 1 (2004).
[17] *GEANT: Detector Description and Simulation Tool* (CERN, Geneva, 1993).